JACS
JOURNAL OF THE AMERICAN CHEMICAL SOCIETY
pubs.acs.org/JACS
Article

Computational Studies of Reactions of 1,2,4,5-Tetrazines with Enamines in MeOH and HFIP

Pengchen Ma,* Dennis Svatunek, Zixi Zhu, Dale L. Boger, Xin-Hua Duan, and K. N. Houk*

Cite This: J. Am. Chem. Soc. 2024, 146, 18706−18713
Read Online
ACCESS | Metrics & More | Article Recommendations | Supporting Information

ABSTRACT: The reaction between 1,2,4,5-tetrazines and alkenes in polar solvents proceeds through a Diels−Alder cycloaddition along the C−C axis (C3/C6 cycloaddition) of the tetrazine, followed by dinitrogen loss. By contrast, the reactions of 1,2,4,5-tetrazines with enamines in hexafluoroisopropanol (HFIP) give 1,2,4-triazine products stemming from a formal Diels−Alder addition across the N−N axis (N1/N4 cycloaddition). We explored the mechanism of this interesting solvent effect through DFT calculations in detail and revealed a novel reaction pathway characterized by C−N bond formation, deprotonation, and a 3,3-sigmatropic rearrangement. The participation of an HFIP molecule was found to be crucial to the N1/N4 selectivity over C3/C6 due to the more favored initial C−N bond formation than C−C bond formation.

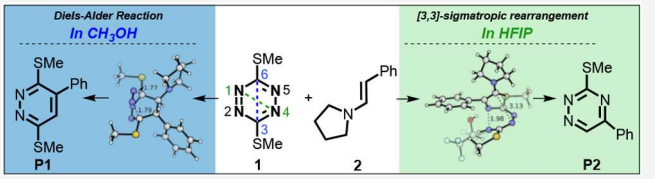

INTRODUCTION

The inverse electron demand Diels−Alder (iEDDA) reaction involving electron-deficient heterocyclic azadienes is a useful strategy for synthesis of highly functionalized heterocycles[1] since it was initially reported by Carboni and Lindsey in 1959.[2] The often very fast cycloaddition between 1,2,4,5-tetrazines and alkenes is now a widely used reaction in bioorthogonal conjugation strategies,[3] synthesis of natural products,[4] modification of metal−organic frameworks,[5] functionalization of carbon nanotubes,[6] and construction of microarrays.[7] Much effort has been devoted to investigating the reactivity and selectivity of these reactions, both experimentally and computationally. Computational studies elucidated their mechanisms, intrinsic reactivities affected by electronic and steric factors, and regio- and stereochemistries.[8] In general, the cycloaddition proceeds across the two carbon atoms (i.e., C3/C6 cycloaddition) of 1,2,4,5-tetrazines, resulting in the formation of a pyridazine product after the loss of N_2 and subsequent aromatization (Scheme 1a).

Recent advancements in this area have been spearheaded by the Boger group.[9] The cycloaddition reactions of 3,6-bis(methylthio)-1,2,4,5-tetrazine (**1**) and 1-styrylpyrrolidine enamine (**2**) are especially interesting because different products are obtained when using different solvents (Scheme 1b). When the reaction is conducted in non-fluorinated solvents such as CH_3OH at 50 °C for 24 h, the conventional C3/C6 cycloaddition product pyridazine **P1** is generated in 66% yield. Strikingly, the use of fluoroalcohol solvents, especially hexafluoroisopropanol (HFIP) at room temperature, resulted in an unprecedented N1/N4 cycloaddition pathway across the N−N axis of the tetrazine. Interesting solvent effects of HFIP have been reported previously.[10] In this case, in HFIP solution, the reaction led to the synthesis of elusive 1,2,4-triazine **P2**, achieving a remarkable 75% yield (Scheme 1b). Experimental mechanistic studies further supported two parallel pathways, one of which generates an isolatable intermediate, **P3**, which could transform to **P2** in HFIP. The structure of **P3** was further confirmed by crystallography, as shown in Figure S1.

We have carried out a comprehensive exploration of the underlying reaction mechanisms using density functional theory (DFT) calculations and established the differing reaction mechanisms in CH_3OH and HFIP.

COMPUTATIONAL DETAILS

DFT calculations were conducted with Gaussian 09.[11] Geometry optimizations and frequency calculations were carried out at the M06-2X[12]/6-31+G(d)[13] level of theory. For solvation effects, the Conductor-Like Polarizable Continuum Model (CPCM)[14] was applied with ε = 32.6 for CH_3OH and ε = 16.7 for HFIP.[15] We have included explicit HFIP in some calculations as well. Vibrational analysis verified the optimized structures as either energy minima or transition states. Single-point energies were subsequently computed on these optimized geometries by using the M06-2X/6-311+G(d,p)−CPCM level. Detailed conformational searches on key intermediates were performed using CREST.[16] Quasiharmonic approximations were employed in the calculations of free

Received: May 6, 2024
Revised: June 11, 2024
Accepted: June 11, 2024
Published: June 28, 2024

https://doi.org/10.1021/jacs.4c06067
J. Am. Chem. Soc. 2024, 146, 18706−18713

Scheme 1. (a) C3/C6 Cycloaddition Diels–Alder Reactions of Tetrazines and Alkenes; (b) Experimental Results of Reactions of Tetrazine 1 and Enamine 2 in CH_3OH or HFIP[9]

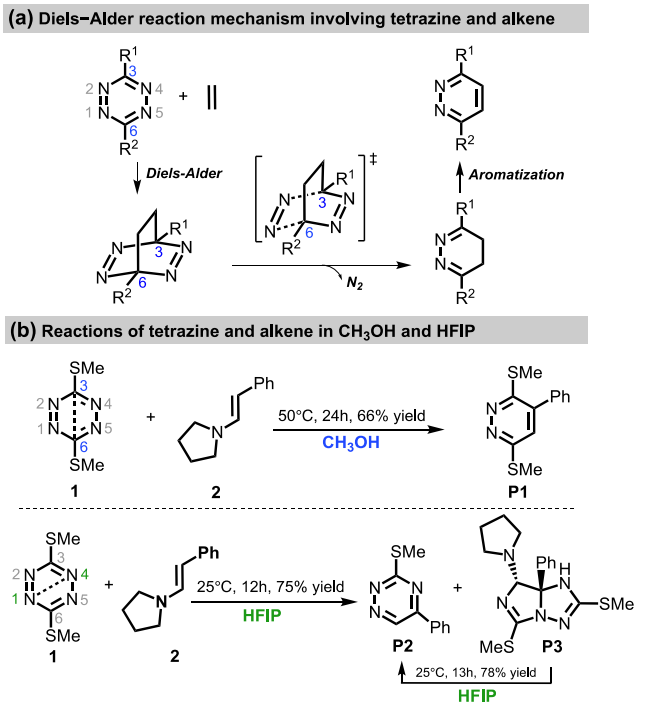

energies using the GoodVibes package.[17] For visualization, all 3D renderings were generated using CYLview[18] or PyMol.[19]

RESULTS AND DISCUSSION

Diazine Product Formed in CH_3OH through C3/C6 Cycloaddition. The cycloaddition between 1,2,4,5-tetrazines and alkenes commonly proceeds through either a concerted or a stepwise Diels–Alder mechanism. Subsequently, a retro-Diels–Alder reaction of N_2 gas and an elimination step yield the aromatic pyridazine products. First, we studied the reaction mechanism of **1** with **2** in implicit CH_3OH. This investigation revealed a stepwise Diels–Alder pathway, corresponding with previous studies.[20] As shown in blue in Figure 1, enamine **2** initially attacks tetrazine **1** at C3 and goes through transition state **3** with a free energy barrier of 21.8 kcal/mol, forming one C–C bond. This leads to a shallow zwitterionic intermediate **4**, 18.4 kcal/mol higher than the starting materials. We have characterized the zwitterionic intermediate **4**, and the Hirshfeld charges on the tetrazine and enamine fragments are −0.31 and +0.31, respectively. Transition state **5** forming the second C–C bond has an energy barrier of only 0.6 kcal/mol. Subsequent retro-Diels–Alder reaction has an energy barrier of 6.7 kcal/mol and provides **8**, which is a very exergonic step involving the extrusion of N_2 gas. Our group earlier explored the rapid dynamics of N_2 extrusion from similar intermediates,[21] the low barrier implies a lifetime of at most a few 100 fs. The final pyridazine product **P1** is formed after elimination of pyrrolidine. The overall reaction is exergonic by −68.7 kcal/mol. When we computed the reaction path in the gas phase, we found that the concerted pathway is favored with the two C–C bonds forming rather synchronously, but the transition state has a free energy barrier of 25.8 kcal/mol due to the absence of stabilization of the zwitterionic transition state and intermediate, shown in Figure S3.

The Gibbs free energy profile of the N1/N4 cycloaddition reaction in implicit CH_3OH solvent is depicted in green in Figure 1. The N1/N4 cycloaddition pathway leading to triazine product **P2** has higher energy barriers than the C3/C6 cycloaddition mechanism (23.3 kcal/mol vs 21.8 kcal/mol, 21.8 kcal/mol vs 19.0 kcal/mol). Corresponding to our previous studies, C–C bond formation is preferred over C–N bond formation in tetrazine cycloadditions.[22] Furthermore, the extrusion of N_2 after the C3/C6 cycloaddition reaction is considerably easier compared to the loss of nitrile after the N1/N4 cycloaddition reaction, with an energy barrier of 15.6

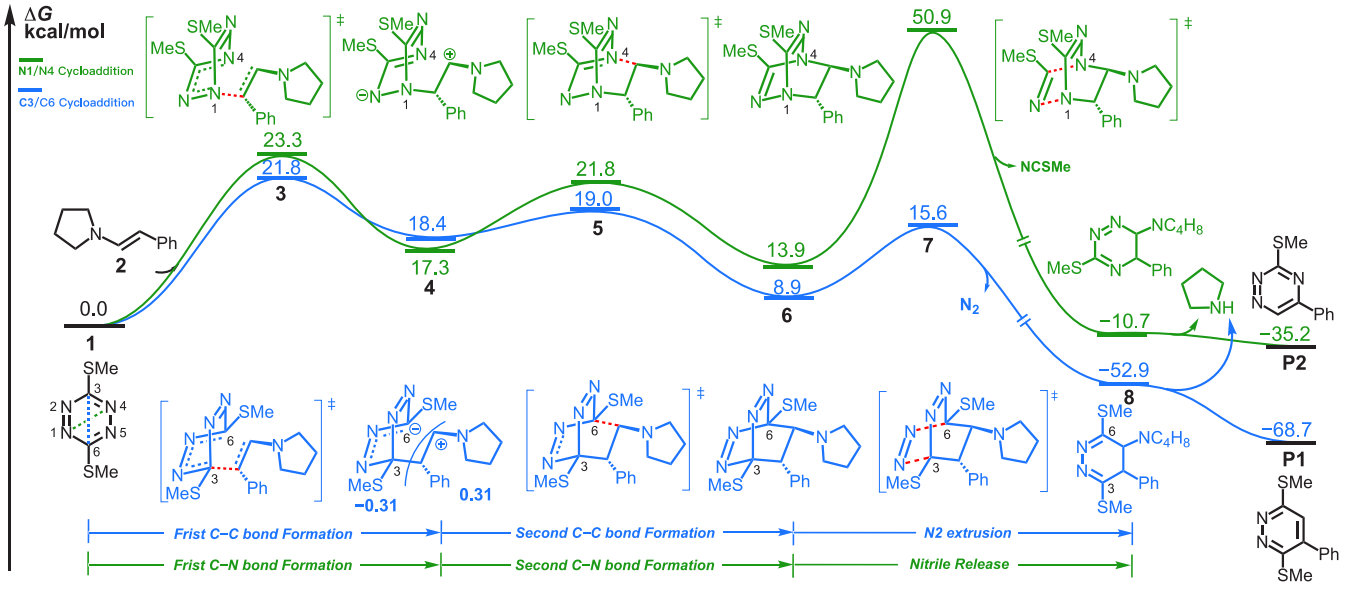

Figure 1. Gibbs free energy profile for C3/C6 cycloaddition (blue) and N1/N4 cycloaddition (green) of tetrazine **1** with enamine **2** in implicit CH_3OH, leading to pyridazine product **P1** and triazine product **P2**, respectively. Hirshfeld charges of zwitterionic species fragments of **4** are shown in bold. We colored the forming and breaking bonds in red.

https://doi.org/10.1021/jacs.4c06067
J. Am. Chem. Soc. 2024, 146, 18706–18713

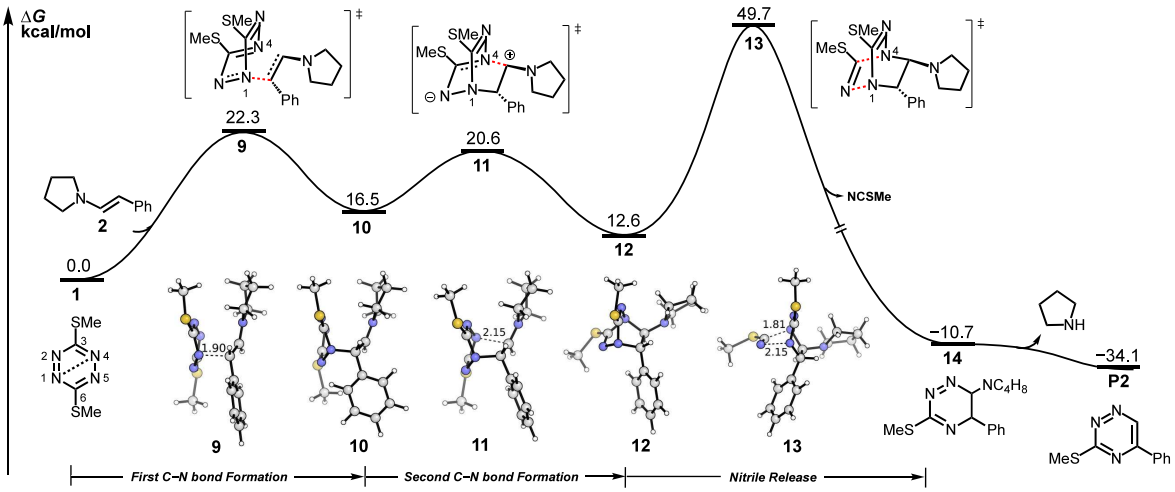

Figure 2. Gibbs free energy profile for the N1/N4 cycloaddition of tetrazine **1** with enamine **2** in implicit HFIP; 3D structures of transition states and key intermediates are shown at the bottom. Distances are in angstroms (Å). We colored the forming and breaking bonds in red.

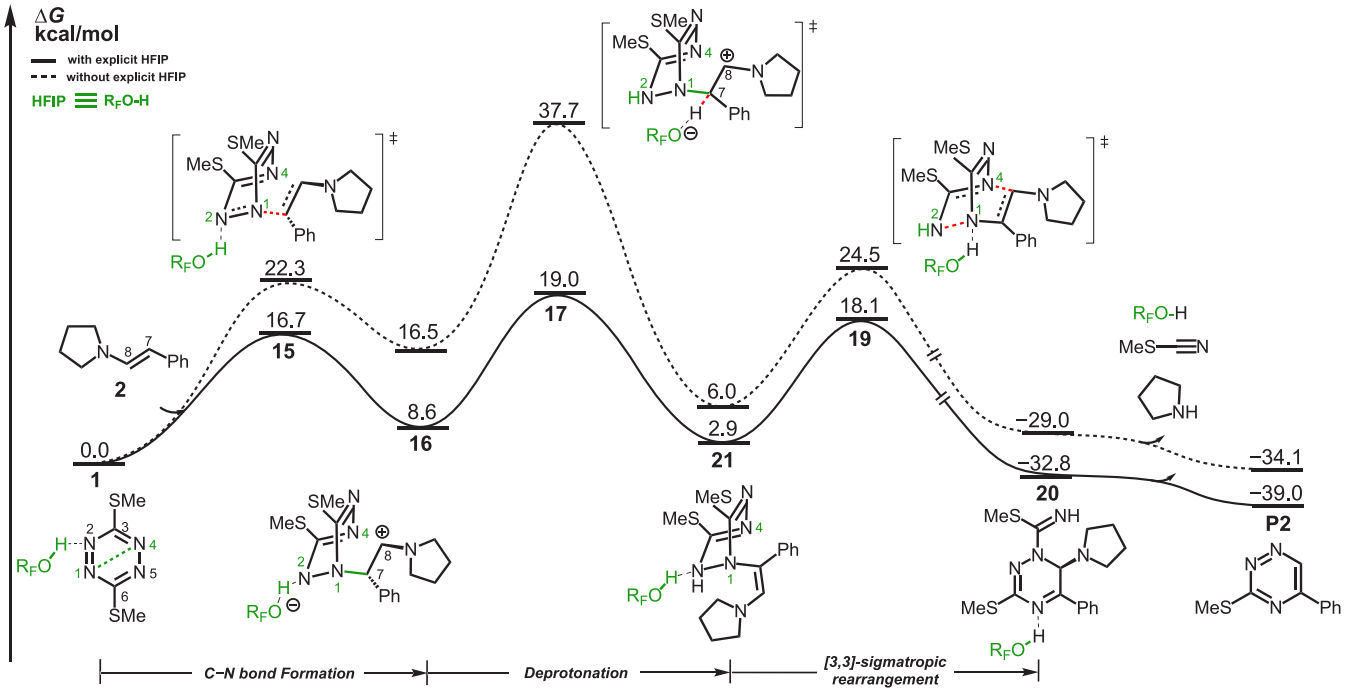

Figure 3. Gibbs free energy profile for N1/N4 cycloaddition of **1** with **2** with (solid line) and without (dashed line) explicit HFIP. 2D structures with HFIP are given. We colored the forming and breaking bonds in red.

kcal/mol vs 50.9 kcal/mol. Notably, the subsequent intermediate **8** after C3/C6 cycloaddition has an exoergic energy of −52.9 kcal/mol, in contrast to −10.7 kcal/mol after release of nitrile; the N_2 extrusion step is thermodynamically favored over the nitrile release by 42.2 kcal/mol. This is consistent with the Evans−Polanyi relationship, since when the reaction becomes more exothermic, the transition state energy is lowered. More specifically, N_2 release involves the cleavage of two weak C−N bonds in exchange for the formation of a strong N≡N bond.[23] 3D structures and bond length information on two transition states **7** are shown in Figure S4.

In CH_3OH, C3/C6 cycloaddition is preferred, giving pyridazine product **P1**. A concerted mechanism occurs in gas phase or in less polar environments,[24] while a polar solvent such as CH_3OH stabilizes the zwitterionic intermediate **4**, leading to a stepwise reaction process.

Reaction in Implicit HFIP through N1/N4 Cycloaddition. The N1/N4 cycloaddition of tetrazine in implicit HFIP is shown in Figure 2, and the energy barrier for the formation of the first C−N bond is 22.3 kcal/mol (**9**), 1.0 kcal/mol lower than the first C−N formation **3** in CH_3OH in Figure 1 in green. Transition state **9** leads to a zwitterionic intermediate **10**, which is more stable than zwitterion **4** in CH_3OH (16.5 kcal/mol in HFIP vs 17.3 kcal/mol in CH_3OH). The second C−N bond formation transition state **11** has a low energy barrier of 4.1 kcal/mol. However, the release of nitrile presents a challenge again, similar in CH_3OH, with a 49.7 kcal/mol energy barrier (**13**). Compared to the N1/N4 cycloaddition in CH_3OH in Figure 1, HFIP facilitates the N1/N4 cycloaddition reaction more efficiently at the beginning of the reaction (C−N bond formations), stabilizing

https://doi.org/10.1021/jacs.4c06067
J. Am. Chem. Soc. 2024, 146, 18706−18713

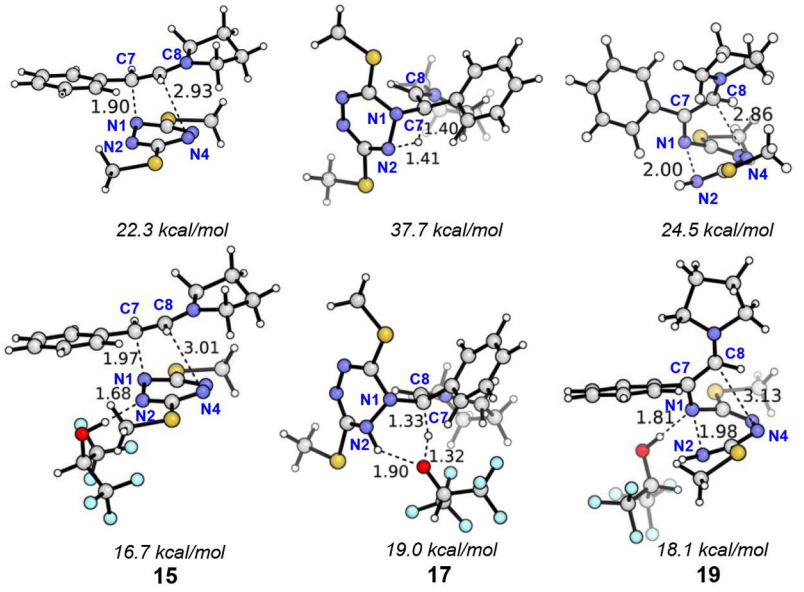

Figure 4. 3D structures and transition states energies of **15**, **17**, and **19** with/without explicit HFIP. Distances are in angstroms (Å).

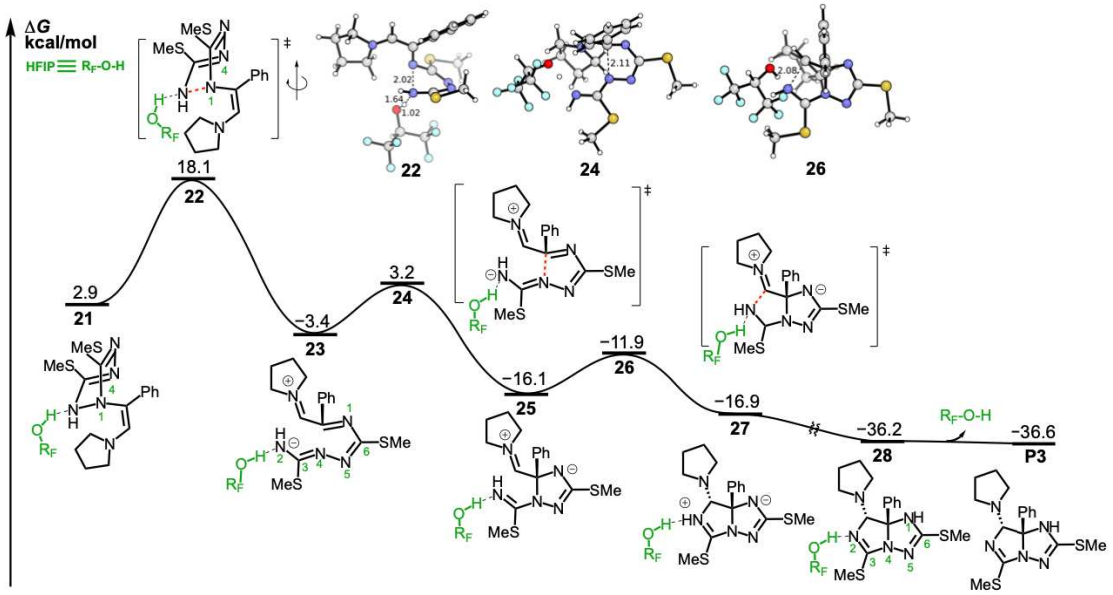

Figure 5. Gibbs free energy profile for the formation of **P3** in HFIP. 3D structures of key transition states **22**, **24**, and **24** are given. Distances are given in angstroms (Å). We colored the forming and breaking bonds in red.

the zwitterionic intermediate **10** but yielding no product **P2** due to the high energy barrier of the last elimination step.

Triazine Product Formed in HFIP through [3,3]-Sigmatropic Rearrangement. We reasoned that HFIP could play an important role in the reaction mechanism that cannot be described correctly by using an implicit solvent model. Therefore, we performed an analysis using explicit HFIP molecules. The reaction profiles with/without explicit HFIP are shown in Figure 3. The HFIP-coordinated tetrazine substrate **1** undergoes attack by enamine at N1 with a 16.7 kcal/mol energy barrier (**15**), lower by 5.6 kcal/mol compared to N1/N4 cycloaddition without explicit HFIP and lower by 1.8 kcal/mol compared to C3/C6 cycloaddition with one explicit HFIP.[25] Zwitterionic species **16** is stabilized by 7.9 kcal/mol with one explicit HFIP. The subsequent deprotonation of C7 has an energy barrier of 10.4 kcal/mol (**17**).[26] Experimental measurements indicate that the reaction (k_{obs} = 6.8 × 10^{-2} L/mol/min) is slightly faster in HFIP than in HFIP-d_2 (k_{obs} = 4.9 × 10^{-2} L/mol/min), which is likely due to decreased acidity of HFIP-d_2.[27] Followed by the isomerization of deprotonated intermediate **18**, a more stable intermediate **21** is formed.[28] Compound **21** goes through a [3,3]-sigmatropic rearrangement transition state **19**, with an energy barrier of 15.2 kcal/mol. This rearrangement involved simultaneous N−N cleavage and the formation of C−N bonds. The intrinsic reaction coordinate (IRC) of **19** is shown in Figure S7. Notably, for the IRC of **19** without explicit HFIP, shown in Figure S7b, N1−N2 breaking is accompanied by C8−N4 formation to form **P2** directly. We did not find computationally the intermediate **d** proposed in Boger's paper.[9] The thermodynamically favored species **20** is formed with an energy of −32.8 kcal/mol. The final aromatization of

https://doi.org/10.1021/jacs.4c06067
J. Am. Chem. Soc. 2024, 146, 18706−18713

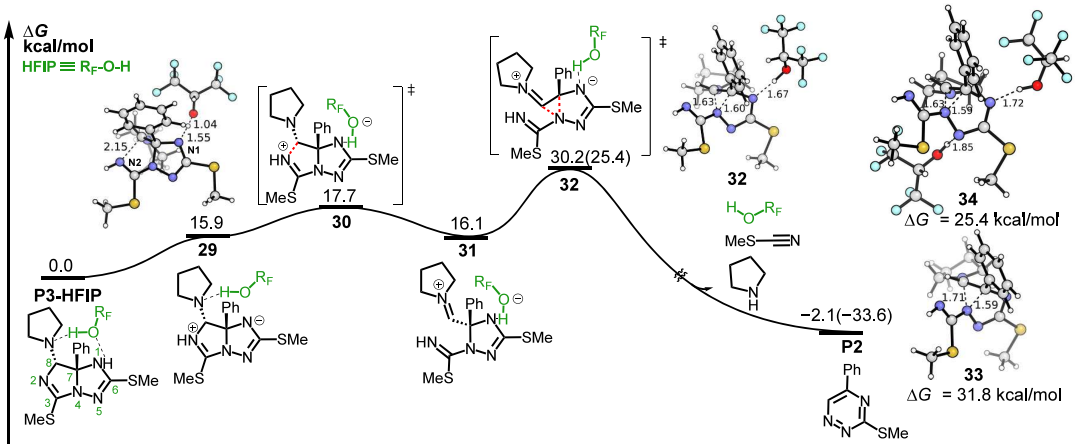

Figure 6. Gibbs free energy profile for the transformation of **P3** to **P2**. 3D transition state structure of the rate-determining step without/one explicit/two explicit HFIP coordinated are shown as **33**, **32**, and **34**, respectively. Distances are in angstroms (Å). We colored the forming and breaking bonds in red.

20 is accompanied by the loss of pyrrolidine and MeSCN, resulting in the formation of the very stable triazine product **P2** with an energy of −39.0 kcal/mol. The corresponding reaction profile with an explicit CH_3OH is shown in Figure S8, where the deprotonation step presents an energy barrier of 33.9 kcal/mol, making it impossible for the [3,3]-sigmatropic rearrangement reaction pathway to happen in CH_3OH.

The participation of explicit HFIP not only lowers the activation energy by stabilizing the charge-separated intermediates but also acts as the proton source. Additionally, the deprotonated HFIP facilitates proton abstraction, which makes a [3,3]-sigmatropic rearrangement feasible. The key transition state structures are shown in Figure 4. Comparing the transition states of C−N bond formation without and with HFIP, **15** benefited from the H-bond interaction of an explicit HFIP molecule. This causes an earlier transition state with a C7−N1 bond formation distance of 1.97 Å (compared to 1.90 Å without the explicit HFIP molecule), reducing the energy barrier by 5.6 kcal/mol. Additionally, the deprotonation process decreased by 18.7 kcal/mol in **17** and activated the N1−N2 bond. This leads to a lower energy barrier in the followed [3,3]-sigmatropic rearrangement transition state **19**. The N1−N2 bond breaking distance is 1.98 Å in transition state **19**, while very little C8−N4 bond formation occurs with a long 3.13 Å distance.

We then investigated the formation of intermediate **P3**. In the experimental studies, compound **P3** was isolated in 36% yield when **1** and enamine **2** were allowed to react in MeOH/HFIP (1:1) solvent mixtures for 2 h. The computed Gibbs free energy profile for this transformation is shown in Figure 5. Started from intermediate **21**, the rate-determining step that proceeds through transition state **22**[29] involves a ring-opening with 15.2 kcal/mol energy barrier, leading to intermediate **23** (−3.4 kcal/mol). The zwitterion species **23** undergoes a 5-endo-trig cyclization with an energy barrier of only 6.6 kcal/mol to give **25**, followed by a 5-exo-trig ring closure with a 4.2 kcal/mol energy barrier to generate **27** (−16.9 kcal/mol). Tautomerization gives compound **28** with an energy of −36.2 kcal/mol. Significantly, the transformation of **23** to **28** is irreversible, with a reversed energy barrier of 39.4 kcal/mol. **P3** is formed by decomplexation at the end. Notably, the transition state energy of **19** leading to **P2** is exactly identical with **22** leading to **P3**; this is in close agreement with experiment result that both **P2** and **P3** are detected in the experimental mechanism study.

Finally, we investigated the experimental findings that in HFIP **P3** converts to **P2** in 13 h and 78% yield at room temperature. As shown in Figure S10, without an explicit HFIP molecule coordinated, the energy barrier of the rate-determining step **48**, which is a ring expansion process, has a height of 31.8 kcal/mol. This corresponds with the experiment result that the transformation from **P3** to **P2** does not occur without HFIP. With one explicit HFIP, **P3-HFIP** undergoes proton transfer and C−N bond cleavage, with the rate-determining step **32** of 30.2 kcal/mol, as shown in Figure 6. When we take two HFIP molecules into consideration to mimic the HFIP solvent environment, we have found that energy barrier of the rate-determining step of ring expansion **34** is decreased to 25.4 kcal/mol, as shown in parentheses in Figure 6. **P2** is given with an exoergic energy of −33.6 kcal/mol. With two H-bonds from two HFIP molecules, transition state **34** presents an early transition state, which has a 1.63 Å forming C−N bond distance and 1.59 Å for the breaking C−N bond. The energy barrier is lowered by 6.4 and 4.8 kcal/mol compared to **33** (without HFIP) or **32** (one explicit HFIP). This finding is in agreement with previous DFT studies that showed that each HFIP molecule lowers the energy barrier by ∼3 kcal/mol.[30] We could imagine that in the real system, where the reaction proceeds in HFIP, with two or more HFIP ions interacted with **P3**, this energy barrier could be even lower than 25.4 kcal/mol.

■ CONCLUSION

Using density functional theory, we unraveled the solvent effect in the reaction between 1,2,4,5-tetrazine and enamine, which leads to an unusual N1/N4 cycloaddition, rather than the common C3/C6 cycloaddition. In polar solvents, such as methanol, an asynchronous C3/C6 cycloaddition Diels−Alder reaction followed by elimination of N_2 leads to the expected pyridazine product, which was confirmed by our calculations. N1/N4 cycloaddition is possible; however, the formed intermediate would need to eliminate a nitrile to form the triazine product. This barrier was found to be too high to be feasible. Using explicit HFIP solvation, we showed that after one initial C−N bond formation, a proton transfer with subsequent [3,3]-sigmatropic arrangement can provide a low-

https://doi.org/10.1021/jacs.4c06067
J. Am. Chem. Soc. 2024, 146, 18706−18713

energy pathway to observed triazine products. Additionally, we demonstrate how an experimentally observed side product can be formed and subsequently also transformed into the triazine product.

This study into solvent effects leading to unusual cycloadditions provides important insight that might be used to control regioselectivity in similar cycloadditions. Mechanistic studies on substitution effects are ongoing in our group.

■ ASSOCIATED CONTENT

Supporting Information

The Supporting Information is available free of charge at https://pubs.acs.org/doi/10.1021/jacs.4c06067.

Computational reaction profiles, IRC figures, deuteration experiment studies, and Cartesian coordinates of all the optimized structures (PDF)

■ AUTHOR INFORMATION

Corresponding Authors

Pengchen Ma − *Department of Chemistry, School of Chemistry, Xi'an Key Laboratory of Sustainable Energy Material Chemistry and Engineering Research Center of Energy Storage Materials and Devices, Ministry of Education, Xi'an Jiaotong University, Xi'an 710049, China; Department of Chemistry and Biochemistry, University of California, Los Angeles, Los Angeles, California 90095, United States;* orcid.org/0000-0002-4110-4696; Email: mapengchen2020@gmail.com

K. N. Houk − *Department of Chemistry and Biochemistry, University of California, Los Angeles, Los Angeles, California 90095, United States;* orcid.org/0000-0002-8387-5261; Email: houk@chem.ucla.edu

Authors

Dennis Svatunek − *Department of Chemistry and Biochemistry, University of California, Los Angeles, Los Angeles, California 90095, United States; Institute of Applied Synthetic Chemistry, TU Wien, 1060 Vienna, Austria;* orcid.org/0000-0003-1101-2376

Zixi Zhu − *Department of Chemistry and The Skaggs Institute for Chemical Biology, The Scripps Research Institute, La Jolla, California 92037, United States*

Dale L. Boger − *Department of Chemistry and The Skaggs Institute for Chemical Biology, The Scripps Research Institute, La Jolla, California 92037, United States;* orcid.org/0000-0002-3966-3317

Xin-Hua Duan − *Department of Chemistry, School of Chemistry, Xi'an Key Laboratory of Sustainable Energy Material Chemistry and Engineering Research Center of Energy Storage Materials and Devices, Ministry of Education, Xi'an Jiaotong University, Xi'an 710049, China*

Complete contact information is available at: https://pubs.acs.org/10.1021/jacs.4c06067

Notes

The authors declare no competing financial interest.

■ ACKNOWLEDGMENTS

We are especially thankful for the financial support from the National Natural Science Foundation of China (No. 22103060), China Postdoctoral Science Foundation (No. 2021M702584), the Fundamental Research Funds for the Central Universities, and the National Science Foundation (USA, CHE−2153972). D.S. is grateful to the Austrian Science Funds (FWF) for funding (J4216). D.L.B. acknowledges the support of the US National Institutes of Health (CA42056). K.N.H. and P.M. are thankful for computation resources from Hoffman2 cluster at UCLA and Expanse at SDSC through allocation CHE040014 from the Advanced Cyberinfrastructure Coordination Ecosystem: Services & Support (ACCESS) program. The authors also acknowledge Professor Yike Zou (SJTU), Professor Xiaosong Xue (SIOC), and Qingyang Zhou (UCLA) for thoughtful advice and Nina Strassner's (FAU) assistance.

■ REFERENCES

(1) (a) Zhang, J.; Shukla, V.; Boger, D. L. Inverse Electron Demand Diels−Alder Reactions of Heterocyclic Azadienes, 1-Aza-1,3-Butadienes, Cyclopropenone Ketals, and Related Systems. A Retrospective. *J. Org. Chem.* **2019**, *84*, 9397−9445. (b) Boger, D. L. Diels−Alder Reactions of Heterocyclic Azadienes. Scope and Applications. *Chem. Rev.* **1986**, *86*, 781−793. (c) Boger, D. L. Diels−Alder Reactions of Azadienes. *Tetrahedron* **1983**, *39*, 2869−2939.

(2) Carboni, R. A.; Lindsey, R. V. Reactions of Tetrazines with Unsaturated Compounds. A New Synthesis of Pyridazines. *J. Am. Chem. Soc.* **1959**, *81*, 4342−4346.

(3) (a) Oliveira, B.; Guo, Z.; Bernardes, G. Inverse Electron Demand Diels−Alder Reactions in Chemical Biology. *Chem. Soc. Rev.* **2017**, *46*, 4895−4950. (b) Png, Z. M.; Zeng, H.; Ye, Q.; Xu, J. Inverse Electron Demand Diels−Alder Reactions: Principles and Applications. *Chem. -Asian J.* **2017**, *12*, 2142−2159. (c) Wu, H.; Devaraj, N. K. Inverse Electron Demand Diels−Alder Bioorthogonal Reactions. In *Cycloadditions in Bioorthogonal Chemistry*; Vrabel, M., Carell, T., Eds.; Springer: Cham, Switzerland, 2016; pp 109−130. (d) Knall, A.-C.; Slugovc, C. Inverse Electron Demand Diels−Alder (iEDDA)-initiated Conjugation: A (High) Potential Click Chemistry Scheme. *Chem. Soc. Rev.* **2013**, *42*, 5131−5142. (e) Blackman, M. L.; Royzen, M.; Fox, J. M. Tetrazine Ligation: Fast Bioconjugation Based on Inverse-Electron-Demand Diels−Alder Reactivity. *J. Am. Chem. Soc.* **2008**, *130*, 13518−13519.

(4) (a) Fu, L.; Gribble, G. W. Total Synthesis of Lycogarubin C Utilizing the Kornfeld−Boger Ring Contraction. *Tetrahedron Lett.* **2010**, *51*, 537−539. (b) Oakdale, J. S.; Boger, D. L. Total Synthesis of Lycogarubin C and Lycogalic Acid. *Org. Lett.* **2010**, *12*, 1132−1134. (c) Hamasaki, A.; Zimpleman, J. M.; Hwang, I.; Boger, D. L. Total Synthesis of Ningalin D. *J. Am. Chem. Soc.* **2005**, *127*, 10767−10770. (d) Boger, D. L.; Hong, J. Asymmetric Total Synthesis of ent-(−)-Roseophilin: Assignment of Absolute Configuration. *J. Am. Chem. Soc.* **2001**, *123*, 8515−8519. (e) Boger, D. L.; Zhang, M. Total Synthesis of (±)-cis and (±)-trans-trikentrin A: Diels−Alder Reactions of Heteroaromatic Azadienes. *J. Am. Chem. Soc.* **1991**, *113*, 4230−4234.

(5) Chen, C.; Allen, C. A.; Cohen, S. M. Tandem Postsynthetic Modification of Metal−Organic Frameworks Using an Inverse-Electron-Demand Diels−Alder Reaction. *Inorg. Chem.* **2011**, *50*, 10534−10536.

(6) (a) Zhu, J.; Hiltz, J.; Lennox, R. B.; Schirrmacher, R. Chemical Modification of Single Walled Carbon Nanotubes with Tetrazine-tethered Gold Nanoparticles via A Diels−Alder Reaction. *Chem. Commun.* **2013**, *49*, 10275−10277. (b) Hayden, H.; Gun'ko, Y. K.; Perova, T.; Grudinkin, S.; Moore, A.; Obraztsova, E. D. Investigation of Tetrazine Functionalised Single Walled Carbon Nanotubes. *Plast. Rubber Compos.* **2009**, *38*, 253−256. (c) Hayden, H.; Gun'ko, Y. K.; Perova, T. S. Chemical Modification of Multi-walled Carbon Nanotubes Using A Tetrazine Derivative. *Chem. Phys. Lett.* **2007**, *435*, 84−89.

(7) (a) Zhang, C.-J.; Tan, C. Y. J.; Ge, J.; Na, Z.; Chen, G. Y. J.; Uttamchandani, M.; Sun, H.; Yao, S. Q. Preparation of Small-Molecule Microarrays by trans-Cyclooctene Tetrazine Ligation and Their Application in the High-Throughput Screening of Protein−

Protein Interaction Inhibitors of Bromodomains. *Angew. Chem., Int. Ed.* **2013**, *52*, 14060−14064. (b) Beckmann, H. S. G.; Niederwieser, A.; Wiessler, M.; Wittmann, V. Preparation of Carbohydrate Arrays by Using Diels−Alder Reactions with Inverse Electron Demand. *Chem.—Eur. J.* **2012**, *18*, 6548−6554.

(8) (a) Houszka, N.; Mikula, H.; Svatunek, D. Substituent Effects in Bioorthogonal Diels−Alder Reactions of 1,2,4,5-Tetrazines. *Chem. − Eur. J.* **2023**, *29*, No. e202300345. (b) Svatunek, D.; Wilkovitsch, M.; Hartmann, L.; Houk, K. N.; Mikula, H. Uncovering the Key Role of Distortion in Bioorthogonal Tetrazine Tools That Defy the Reactivity/Stability Trade-Off. *J. Am. Chem. Soc.* **2022**, *144*, 8171−8177. (c) Kamber, D. N.; Nguyen, S. S.; Liu, F.; Briggs, J. S.; Shih, H.-W.; Row, R. D.; Long, Z. G.; Houk, K. N.; Liang, Y.; Prescher, J. A. Isomeric Triazines Exhibit Unique Profiles of Bioorthogonal Reactivity. *Chem. Sci.* **2019**, *10*, 9109−9114. (d) Yang, Y.-F.; Liang, Y.; Liu, F.; Houk, K. N. Diels−Alder Reactivities of Benzene, Pyridine, and Di-, Tri-, and Tetrazines: The Roles of Geometrical Distortions and Orbital Interactions. *J. Am. Chem. Soc.* **2016**, *138*, 1660−1667. (e) Talbot, A.; Devarajan, D.; Gustafson, S. J.; Fernández, I.; Bickelhaupt, F. M.; Ess, D. H. Activation-Strain Analysis Reveals Unexpected Origin of Fast Reactivity in Heteroaromatic Azadiene Inverse-Electron-Demand Diels−Alder Cycloadditions. *J. Org. Chem.* **2015**, *80*, 548−558. (f) Liu, F.; Liang, Y.; Houk, K. N. Theoretical Elucidation of the Origins of Substituent and Strain Effects on the Rates of Diels−Alder Reactions of 1,2,4,5-Tetrazines. *J. Am. Chem. Soc.* **2014**, *136*, 11483−11493.

(9) Zhu, Z.; Glinkerman, C. M.; Boger, D. L. Selective N1/N4 N1/N4 cycloaddition of 1,2,4,5-Tetrazines Enabled by Solvent Hydrogen Bonding. *J. Am. Chem. Soc.* **2020**, *142*, 20778−20787.

(10) (a) Zhao, X.; Hu, X.; Lv, X.; Wu, Y.-B.; Bu, Y.; Lu, G. How Hexafluoroisopropanol Solvent promotes Diels−Alder Cycloadditions: ab initiometadynamics Simulations. *Phys. Chem. Chem. Phys.* **2023**, *25*, 14695−14699. (b) Hu, X.; Zhao, X.; Lv, X.; Wu, Y.-B.; Bu, Y.; Lu, G. Ab Initio Metadynamics Simulations of Hexafluoroisopropanol Solvent Effects: Synergistic Role of Solvent H-Bonding Networks and Solvent-Solute C-H/π interactions. *Chem.—Eur. J.* **2023**, *29*, No. e202203879. (c) Motiwala, H. F.; Armaly, A. M.; Cacioppo, J. G.; Coombs, T. C.; Koehn, K. R. K.; Norwood, V. M., IV; Aubé, J. HFIP in Organic Synthesis. *Chem. Rev.* **2022**, *122*, 12544−12747. (d) Colomer, I.; Chamberlain, A. E. R.; Haughey, M. B.; Donohoe, T. J. Hexafluoroisopropanol as a Highly Versatile Solvent. *Nat. Rev. Chem.* **2017**, *1*, 0088.

(11) Frisch, M. J.; Trucks, G. W.; Schlegel, H. B.; Scuseria, G. E.; Robb, M. A.; Cheeseman, J. R.; Scalmani, G.; Barone, V.; Mennucci, B.; Petersson, G. A.; Nakatsuji, H.; Caricato, M.; Li, X.; Hratchian, H. P.; Izmaylov, A. F.; Bloino, J.; Zheng, G.; Sonnenberg, J. L.; Hada, M.; Ehara, M.; Toyota, K.; Fukuda, R.; Hasegawa, J.; Ishida, M.; Nakajima, T.; Honda, Y.; Kitao, O.; Nakai, H.; Vreven, T.; Montgomery, J. A., Jr.; Peralta, J. E.; Ogliaro, F.; Bearpark, M.; Heyd, J. J.; Brothers, E.; Kudin, K. N.; Staroverov, V. N.; Keith, T.; Kobayashi, R.; Normand, J.; Raghavachari, K.; Rendell, A.; Burant, J. C.; Iyengar, S. S.; Tomasi, J.; Cossi, M.; Rega, N.; Millam, J. M.; Klene, M.; Knox, J. E.; Cross, J. B.; Bakken, V.; Adamo, C.; Jaramillo, J.; Gomperts, R.; Stratmann, R. E.; Yazyev, O.; Austin, A. J.; Cammi, R.; Pomelli, C.; Ochterski, J. W.; Martin, R. L.; Morokuma, K.; Zakrzewski, V. G.; Voth, G. A.; Salvador, P.; Dannenberg, J. J.; Dapprich, S.; Daniels, A. D.; Farkas, O.; Foresman, J. B.; Ortiz, J. V.; Cioslowski, J.; Fox, D. J. *Gaussian 09, revision D.01*; Gaussian Inc.: Wallingford, CT, 2013.

(12) (a) Zhao, Y.; Truhlar, D. G. The M06 Suite of Density Functionals for Main Group Thermochemistry, Thermochemical Kinetics, Noncovalent Interactions, Excited States, and Transition Elements: Two New Functionals and Systematic Testing of Four M06-Class Functionals and 12 Other Functionals. *Theor. Chem. Acc.* **2008**, *120*, 215−241. (b) Zhao, Y.; Truhlar, D. G. Density Functionals with Broad Applicability in Chemistry. *Acc. Chem. Res.* **2008**, *41*, 157−167.

(13) (a) Hariharan, P. C.; Pople, J. A. The Influence of Polarization Functions on Molecular Orbital Hydrogenation Energies. *Theor. Chim. Acta* **1973**, *28*, 213−222. (b) Hehre, W. J.; Ditchfield, R.; Pople, J. A. Self—Consistent Molecular Orbital Methods. XII. Further Extensions of Gaussian—Type Basis Sets for Use in Molecular Orbital Studies of Organic Molecules. *J. Chem. Phys.* **1972**, *56*, 2257−2261. (c) Ditchfield, R.; Hehre, W. J.; Pople, J. A. Self-Consistent Molecular-Orbital Methods. IX. An Extended Gaussian-Type Basis for Molecular-Orbital Studies of Organic Molecules. *J. Chem. Phys.* **1971**, *54*, 724−728.

(14) (a) Takano, Y.; Houk, K. N. Benchmarking the Conductor-like Polarizable Continuum Model (CPCM) for Aqueous Solvation Free Energies of Neutral and Ionic Organic Molecules. *J. Chem. Theory Comput.* **2005**, *1*, 70−77. (b) Cossi, M.; Rega, N.; Scalmani, G.; Barone, V. Energies, Structures, and Electronic Properties of Molecules in Solution with the C-PCM Solvation Model. *J. Comput. Chem.* **2003**, *24*, 669−681. (c) Barone, V.; Cossi, M. J. Quantum Calculation of Molecular Energies and Energy Gradients in Solution by a Conductor Solvent Model. *Phys. Chem. A* **1998**, *102*, 1995−2001. (d) We have tested the SMD solvent model, and the results are shown in Figure S2.

(15) HFIP parameters used in calculation: eps = 16.7, epsinf = 1.625625, HBondAcidity = 1.96, HBondBasicity = 0.00, SurfaceTensionAtInterface = 23.2306248, CarbonAromaticity = 0.0, and ElectronegativeHalogenicity = 0.60

(16) Pracht, P.; Bohle, F.; Grimme, S. Automated Exploration of the Low-Energy Chemical Space with Fast Quantum Chemical Methods. *Phys. Chem. Chem. Phys.* **2020**, *22*, 7169−7192.

(17) (a) Luchini, G.; Alegre-Requena, J. V.; Funes-Ardoiz, I.; Paton, R. S. GoodVibes: automated thermochemistry for heterogeneous computational chemistry data. *F1000Research* **2020**, *9*, 291. (b) Grimme, S. Supramolecular Binding Thermodynamics by Dispersion-Corrected Density Functional Theory. *Chem.—Eur. J.* **2012**, *18*, 9955−9964. (c) We calculated energies under each experimental reaction temperature, with 1 mol/L concentration.

(18) Legault, C. Y. CYLview20 ; Université de Sherbrooke: 2020 (http://www.cylview.org).

(19) *The PyMOL Molecular Graphics System*, version 3.0, Schrödinger, LLC.

(20) Yang, Y.-F.; Yu, P.; Houk, K. N. Computational Exploration of Concerted and Zwitterionic Mechanisms of Diels−Alder Reactions between 1,2,3-Triazines and Enamines and Acceleration by Hydrogen-Bonding Solvents. *J. Am. Chem. Soc.* **2017**, *139*, 18213−18221.

(21) Törk, L.; Jiménez-Osés, G.; Doubleday, C.; Liu, F.; Houk, K. N. Molecular Dynamics of the Diels-Alder Reactions of Tetrazines with Alkenes and N_2 Extrusions from Adducts. *J. Am. Chem. Soc.* **2015**, *137*, 4749−4758.

(22) (a) Yu, S.; de Bruijn, H. M.; Svatunek, D.; Hamlin, T. A.; Bickelhaupt, F. M. Factors Controlling the Diels−Alder Reactivity of Hetero-1,3-Butadienes. *ChemistryOpen.* **2018**, *7*, 995−1004. (b) Liu, F.; Liang, Y.; Houk, K. N. Bioorthogonal Cycloadditions: Computational Analysis with the Distortion/Interaction Model and Predictions of Reactivities. *Acc. Chem. Res.* **2017**, *50*, 2297−2308.

(23) Related bond dissociation energies: C−N 69 kcal/mol, N≡N 226 kcal/mol, C−C 82 kcal/mol, C−O 87 kcal/mol, C═O 177 kcal/mol.

(24) (a) In gas phase: reference 21. Calculations of C3/C6 cycloaddition in the gas phase in Figure S3. (b) In less polar environment: Suh, S.-E.; Chen, S.; Houk, K. N.; Chenoweth, D. M. The mechanism of the triple aryne−tetrazine reaction cascade: theory and experiment. *Chem. Sci.* **2018**, *9*, 7688−7693.

(25) Transition state energy and structure of first C−C bond formation with one explicit HFIP in C3/C6 cycloaddition, shown in Figure S5.

(26) For the proton transfer process in our calculations, tunneling behavior was estimated with the correction by Skodje and co-workers using the PyTUN utility (https://github.com/SJ-Ang/PyTUN).

(27) (a) For investigation of the reactions in deuterated-HFIP, see Part 2 in Supporting Information. (b) Perrin, C. L.; Dong, Y. Secondary Deuterium Isotope Effects on the Acidity of Carboxylic Acids and Phenols. *J. Am. Chem. Soc.* **2007**, *129*, 4490−4497.

https://doi.org/10.1021/jacs.4c06067
J. Am. Chem. Soc. 2024, 146, 18706−18713

(28) Isomerization structures and energies of **18** and **21** are shown in Figure S6.
(29) The comparison of Gibbs free energy of HFIP molecule coordinated to N2 and N4 in the rate-determining step of **P2** transformed to **P3**, shown in Figure S9.
(30) Zhou, Y.; Xue, R.; Feng, Y.; Zhang, L. How Does HOTf/HFIP Cooperative System Catalyze the Ring-Opening Reaction of Cyclopropanes? A DFT Study. *Asian J. Org. Chem.* **2020**, *9*, 311−316.

https://doi.org/10.1021/jacs.4c06067
J. Am. Chem. Soc. 2024, 146, 18706−18713